2040 *Organometallics* **2010,** *29,* 2040–2045
DOI: 10.1021/om1000315

ORGANOMETALLICS
Article

Mechanism for Hydride-Assisted Rearrangement from Ethylidene to Ethylene in Iridium Cationic Complexes

Maria Besora,[†,‡] Sergei F. Vyboishchikov,[§] Agustí Lledós,[‡] Feliu Maseras,*[,†,‡] Ernesto Carmona,[⊥] and Manuel L. Poveda[⊥]

[†]*Institute of Chemical Research of Catalonia (ICIQ), Avinguda Països Catalans 16, 43007 Tarragona, Catalonia, Spain,* [‡]*Departament de Química, Edifici Cn, Universitat Autònoma de Barcelona, 08193 Bellaterra, Catalonia, Spain,* [§]*Institut de Química Computacional, Campus de Montilivi, Universitat de Girona, 17071 Girona, Catalonia, Spain, and* [⊥]*Instituto de Investigaciones Químicas and Departamento de Química Inorgánica, Consejo Superior de Investigaciones Científicas and Universidad de Sevilla, Avenida Américo Vespucio 49, 41092 Sevilla, Spain*

Received January 11, 2010

The cationic hydride alkylidene complexes $[Tp^{Me_2}Ir(=CH-CH_3)(H)(PMe_3)]^+$ and $[Cp^*Ir(=CH-CH_3)(H)(PMe_3)]^+$ (Tp^{Me_2} = hydrotris(3,5-dimethyl-1-pyrazolyl)borate; Cp* = pentamethylcyclopentadienyl) are experimentally known to tautomerize to the corresponding hydride alkene species. Our computational study on the mechanism shows that the reaction takes place through formation of the corresponding alkyl intermediates, with participation of species involving α- and β-CH agostic interactions. Computed energy barriers reproduce the available experimental kinetic data and agree with a much faster process in the Cp* system. The highest stabilization of the hydride alkylidene complex (the reactant) in the Tp^{Me_2} system appears as the main reason for the higher barrier found. The difference between the two complexes is due to the steric effects of the spectator ligands.

Introduction

Ligand conversions through hydrogen migration in the coordination sphere of transition metal complexes participate in a large number of common chemical processes, such as α-C−H and β-C−H additions and eliminations.[1,2] Some of the species that may interconvert by means of these processes are transition metal carbene, alkyl, and π-alkene complexes, which are essential intermediates in many organometallic reactions.[3,4]

The isomerization of a hydride−alkylidene complex $L_n(H)M(=C(H)-CR_2H)$ to give the corresponding alkene π-complex $L_n(H)M(\eta^2\text{-}CH_2{=}CR_2)$ is well documented for cationic electrophilic complexes.[5,6] The reverse process is known to take place in early transition metal species,[7−10] and in some cases the equilibrium between both complexes has been observed.[6,11,12] A typical reaction sequence is shown in Scheme 1. A hydride alkenyl complex is protonated, resulting in hydride alkylidene species **a**/**A** (labeling scheme explained below), which evolves to the hydride alkene **e**/**E**. The presence of a metal−alkyl intermediate seems to be general,[13] and the process involves migration of the hydride to the alkylidene and β-hydrogen elimination steps.[13−17] The mechanism is further complicated by the possible existence of different alkyl intermediates: α-agostic (**b**/**B**), nonagostic (**c**/**C**), or β-agostic (**d**/**D**) forms.[18−23] The reaction

*Corresponding author. E-mail: fmaseras@iciq.es. Tel: 34 977 920 202. Fax: 34 977 920 231.

(1) Chirik, P. J.; Bercaw, J. E. *Organometallics* **2005**, *24*, 5407–5423.
(2) Davies, H. M. L; Long, M. S. *Angew. Chem., Int. Ed.* **2005**, *44*, 3518–3520.
(3) Diaz-Requejo, M. M.; Perez, P. J. *Chem. Rev.* **2008**, *108*, 3379–3394.
(4) Esteruelas, M. A.; Lopez, A. M.; Olivan, M. *Coord. Chem. Rev.* **2007**, *251*, 795–840.
(5) Brookhart, M.; Tucker, J. R.; Husk, G. R. *J. Am. Chem. Soc.* **1981**, *103*, 979–981.
(6) Paneque, M.; Poveda, M. L.; Santos, L. L.; Carmona, E.; Lledos, A.; Ujaque, G.; Mereiter, K. *Angew. Chem., Int. Ed.* **2004**, *43*, 3708–3711.
(7) Freundlich, J. S.; Schrock, R. R.; Davis, W. M. *J. Am. Chem. Soc.* **1996**, *118*, 3643–3655.
(8) Giannini, L.; Guillemot, G.; Solari, E.; Floriani, C.; Re, N.; Chiesi-Villa, A.; Rizzoli, C. *J. Am. Chem. Soc.* **1999**, *121*, 2797–2807.
(9) Hirsekorn, K. F.; Veige, A. S.; Marshak, M. P.; Koldobskaya, Y.; Wolczanski, P. T.; Cundari, T. R.; Lobkovsky, E. B. *J. Am. Chem. Soc.* **2005**, *127*, 4809–4830.
(10) Ozerov, O. V.; Watson, L. A.; Pink, M.; Caulton, K. G. *J. Am. Chem. Soc.* **2003**, *125*, 9604–9605.
(11) Fellmann, J. D.; Schrock, R. R.; Traficante, D. D. *Organometallics* **1982**, *1*, 481–484.
(12) Parkin, G.; Bunel, E.; Burger, B. J.; Trimmer, M. S.; Vanasselt, A.; Bercaw, J. E. *J. Mol. Catal.* **1987**, *41*, 21–39.
(13) Carmona, E.; Paneque, M.; Poveda, M. L. *Dalton Trans.* **2003**, 1–8.
(14) Ingleson, M. J.; Yang, X. F.; Pink, M.; Caulton, K. G. *J. Am. Chem. Soc.* **2005**, *127*, 10846–10847.
(15) Kuznetsov, V. F.; Abdur-Rashid, K.; Lough, A. J.; Gusev, D. G. *J. Am. Chem. Soc.* **2006**, *128*, 14388–14396.
(16) Ozerov, O. V.; Watson, L. A.; Pink, M.; Caulton, K. G. *J. Am. Chem. Soc.* **2007**, *129*, 6003–6016.
(17) Rankin, M. A.; McDonald, R.; Ferguson, M. J.; Stradiotto, M. *Angew. Chem., Int. Ed.* **2005**, *44*, 3603–3606.
(18) Brookhart, M.; Green, M. L. H. *J. Organomet. Chem.* **1983**, *250*, 395–408.
(19) Brookhart, M.; Green, M. L. H.; Wong, L.-L. *Prog. Inorg. Chem.* **1988**, *36*, 1–124.
(20) Etienne, M.; McGrady, J. E.; Maseras, F. *Coord. Chem. Rev.* **2009**, *253*, 635–646.
(21) Fryzuk, M. D.; Johnson, S. A.; Rettig, S. J. *J. Am. Chem. Soc.* **2001**, *123*, 1602–1612.

 Published on Web 04/14/2010

Scheme 1. Proposed Reaction Mechanism for the Rearrangement between Hydride Alkylidene and Hydride Alkene Complexes

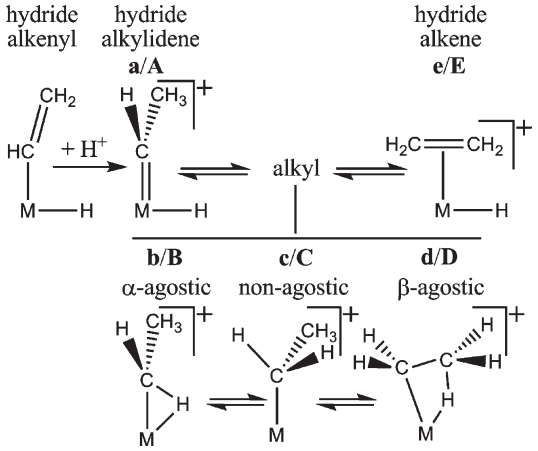

mechanism is interesting by itself, and it can moreover provide insight into the intimately related alkene insertion step in metallocene polymerization catalysis, where the new bond is not C−H but C−C.[24−26]

Experimental and computational studies on these rearrangements have illustrated the mechanistic complexity. For Tp^{Me_2}-Ir(H)(*o*-C_6H_4(O)C(CH_3)=),[6,27] it has been shown that the rate-limiting step is the isomerization between both agostic intermediates. For [PC═CP]RuHCl[15] (PC═CP = *N*,*N*′-bis-(di-*tert*-butylphosphino)-1,3-diaminoprop-1-ene) and for $(H)_2Zr$═$CHCH_3$,[28] the α-H elimination is the rate-limiting step. Other computational work has found that all the possible agostic intermediates need not necessarily be present.[29−32] The alkene−alkylidene rearrangement has also been shown to take place without assistance of hydride ligands.[33]

In this paper we present a computational study of the rearrangement mechanism for two different iridium complexes: $[Tp^{Me_2}Ir(=CH-CH_3)(H)(PMe_3)]^+$ and $[Cp^*Ir(=CH-CH_3)(H)(PMe_3)]^+$. For the $[Tp^{Me_2}Ir(CH=CH_2)(H)(PMe_3)]$ system there are detailed kinetic experimental data available.[34] By monitoring the disappearance of the cationic hydride−ethylidene complex at −47 °C, a $\Delta^{\ddagger}G^{\circ}_{226}$ of 16.7 kcal·mol^{-1} was measured, corresponding to the barrier of the rate-determining step of the whole process, from **a**/**A** to **e**/**E**. Additional experiments with deuterated species allowed for deeper insight into the mechanism. Deuteration of the **e**/**E** product in CD_3OD, which is assumed to take place through reactants **a**/**A** (requiring the inverse reaction to occur), has a $\Delta^{\ddagger}G^{\circ}_{298}$ barrier of 25.1 kcal·mol^{-1}. The scrambling between deuterium and hydrogen atoms of alkene and hydride in **e**/**E** was measured to take place with a $\Delta^{\ddagger}G^{\circ}_{273}$ of 21.1 kcal·mol^{-1}, attributed to the *β*-H addition step **e**/**E** from **d**/**D**. Assuming a small temperature dependence of the barriers, some indirect data can be estimated: (i) $\Delta^{\ddagger}G^{\circ}_{226}$ of 16.7 kcal·mol^{-1} from **a**/**A** to **e**/**E** and $\Delta^{\ddagger}G^{\circ}_{298}$ of 25.1 kcal·mol^{-1} for the reverse process lead to a reaction exergonicity close to 8 kcal·mol^{-1}. (ii) $\Delta^{\ddagger}G^{\circ}_{298}$ of 25.1 kcal·mol^{-1} from **e**/**E** to **a**/**A** and $\Delta^{\ddagger}G^{\circ}_{273}$ of 21.1 kcal·mol^{-1} from **e**/**E** to **d**/**D** lead to the estimation that the energy of the transition state between **d**/**D** and **e**/**E** must be about 4 kcal·mol^{-1} below the rate-determining step for the whole process. The reaction of $[Cp^*Ir(=CH-CH_3)(H)(PMe_3)]^+$ was experimentally studied by similar procedures,[13] although the protonation of the hydride−vinyl complex is fast and elucidation of Gibbs energies or detection of intermediates was not possible.

The goal of the present work is twofold. On one hand, we want to validate the general mechanism presented in Scheme 1 and to elucidate the role of alkyl intermediates in the particular case of $[Tp^{Me_2}Ir(=CH-CH_3)(H)(PMe_3)]^+$, for which many experimental data are available. On the other hand, we want to understand the difference between the rates for the two complexes. Comparisons between Tp- and Cp-type ligands can be found regarding H_2 activation, showing that Cp ligands favor the oxidative addition due to the stronger electron-donor character of Cp compared with Tp.[35−37] In our case, the reaction is faster for Cp*, contrary to the expectation that this more electron-donating ligand[38] should stabilize the carbene, thus slowing the reaction. In our studies, density functional theory (DFT) was used to examine the two complexes of interest. The species presented are named according to the labels in Scheme 1. Lowercase letters **a**−**e** are used for the $[Tp^{Me_2}Ir(=CH-CH_3)(H)(PMe_3)]^+$ system, and capital letters **A**−**E** for the $[Cp^*Ir(=CH-CH_3)(H)(PMe_3)]^+$ system. The starting point of our mechanistic study will be the hydride−alkylidene complex **a**/**A**, and we will consider its conversion to the hydride alkene complex **e**/**E**. Unless stated otherwise, the computed energies presented throughout the paper include solvation and standard Gibbs energy corrections at 298 K.

Computational Details

Most calculations presented in this paper were carried out with DFT using the B3LYP functional[39−41] as implemented in Gaussian 03.[42] Both systems $[Cp^*Ir(=CH-CH_3)(H)(PMe_3)]^+$ and $Tp^{Me_2}Ir(=CH-CH_3)(H)(PMe_3)]^+$ were treated with the standard split-valence polarized 6-31G(d,p) basis set[43−45] for all the atoms except the metal center. The LANL2TZ(f) valence

(22) Jaffart, J.; Etienne, M.; Maseras, F.; McGrady, J. E.; Eisenstein, O. *J. Am. Chem. Soc.* **2001**, *123*, 6000–6013.
(23) Li, X. W.; Appelhans, L. N.; Faller, J. W.; Crabtree, R. H. *Organometallics* **2004**, *23*, 3378–3387.
(24) Bochmann, M. *J. Organomet. Chem.* **2004**, *689*, 3982–3998.
(25) Natta, G.; Pino, P.; Corradini, P.; Danusso, F.; Mantica, E.; Mazzanti, G.; Moraglio, G. *J. Am. Chem. Soc.* **1955**, *77*, 1708–1710.
(26) Ziegler, K.; Holzkamp, E.; Breil, H.; Martin, H. *Angew. Chem., Int. Ed. Engl.* **1955**, *67*, 426–426.
(27) Lara, P.; Paneque, M.; Poveda, M. L.; Santos, L. L.; Valpuesta, J. E. V.; Salazar, V.; Carmona, E.; Moncho, S.; Ujaque, G.; Lledós, A.; Maya, C.; Mereiter, K. *Chem.—Eur. J.* **2009**, *15*, 9046–9057.
(28) Cho, H. G.; Andrews, L. *J. Phys. Chem. A* **2008**, *112*, 1519–1525.
(29) Coalter, J. N.; Bollinger, J. C.; Huffman, J. C.; Werner-Zwanziger, U.; Caulton, K. G.; Davidson, E. R.; Gerard, H.; Clot, E.; Eisenstein, O. *New J. Chem.* **2000**, *24*, 9–26.
(30) Handzlik, J.; Stosur, M.; Kochel, A.; Szymanska-Buzar, T. *Inorg. Chim. Acta* **2008**, *361*, 502–512.
(31) Ozerov, O. V.; Watson, L. A.; Pink, M.; Caulton, K. G. *J. Am. Chem. Soc.* **2004**, *126*, 6363–6378.
(32) Spencer, L. P.; Beddie, C.; Hall, M. B.; Fryzuk, M. D. *J. Am. Chem. Soc.* **2006**, *128*, 12531–12543.
(33) Castro-Rodrigo, R.; Esteruelas, M. A.; Fuertes, S.; Lopez, A. M.; Mozo, S.; Onate, E. *Organometallics* **2009**, *28*, 5941–5951.
(34) Alias, F. M.; Poveda, M. L.; Sellin, M.; Carmona, E. *J. Am. Chem. Soc.* **1998**, *120*, 5816–5817.
(35) Gelabert, R.; Moreno, M.; Lluch, J. M.; Lledós, A. *Organometallics* **1997**, *16*, 3805–3814.
(36) Jia, G.; Lau, C.-P. *Coord. Chem. Rev.* **1999**, *190−192*, 83–108.
(37) Man, M. L.; Zhu, J.; Ng, S. M.; Zhou, Z. Y.; Yin, C. Q.; Lin, Z. Y.; Lau, C. P. *Organometallics* **2004**, *23*, 6214–6220.
(38) Tellers, D. M.; Skoog, S. J.; Bergman, R. G.; Gunnoe, T. B.; Harman, W. D. *Organometallics* **2000**, *19*, 2428–2432.
(39) Becke, A. D. *J. Chem. Phys.* **1993**, *98*, 5648–5652.
(40) Lee, C. T.; Yang, W. T.; Parr, R. G. *Phys. Rev. B* **1988**, *37*, 785–789.
(41) Stephens, P. J.; Devlin, F. J.; Chabalowski, C. F.; Frisch, M. J. *J. Phys. Chem.* **1994**, *98*, 11623–11627.

basis set[46−48] with the associated effective core potentials[47,49,50] was used for iridium. Frequency calculations were performed to characterize the stationary points. IRC calculations were performed on selected transition states to confirm their connection to the minima. Low-energy conformers associated with rotation of methyl groups of ligands were found in the most sterically crowded complexes. In particular, several conformers within a 1 kcal·mol^{-1} range were found for the hydride alkylidene species. Only the most stable one for each species is discussed in the text.

The solvent effect was taken into account by single-point calculations using the polarizable continuum model (PCM),[51−54] namely, IEF-PCM as implemented in Gaussian 03. Default options were used, except that individual spheres were placed on all hydrogen atoms to get a more accurate cavity. Experimental data had been obtained using a number of solvents: CH_2Cl_2, CD_3OD, and a 4:1 CH_2Cl_2/CD_3OD mixture. In order to relate easily the different steps of the reaction, only one of the experimental solvents, dichloromethane ($\varepsilon = 8.93$), was considered. The standard Gibbs energies in dichloromethane ($\Delta G°_{sol}$) were obtained by adding the solvation energies to the gas-phase Gibbs energies computed at 298 K. Reported experimental $\Delta^{‡}G°_{T}$ data for the Tp^{Me_2} system were obtained at different temperatures, 226, 273, or 298 K. We decided however to use 298 K in all of our calculations because the goal is not reproducing a given experimental barrier but to provide a compatible mechanistic proposal and because $\Delta^{‡}G°_{T}$ is expected to be virtually constant over the considered range of temperatures. The overall entropic contribution of these processes is indeed fairly small (i.e., 0.1 kcal·mol^{-1} at 298 K for the rate-limiting step of the Tp^{Me_2} system).

The spin ground state of the 16-electron alkyl intermediate **c/C** was confirmed to be singlet. The triplet state is 16 kcal·mol^{-1} above the singlet for $[Tp^{Me_2}Ir(CH_2CH_3)(PMe_3)]^+$ and 23 kcal·mol^{-1} for $[Cp^*Ir(CH_2CH_3)(PMe_3)]^+$. Thus, no spin-state crossings are expected to take place, and singlet species are considered only further on.

Scheme 2. Schematic Representation of the Rearrangement of the Hydride−Ethylidene Complex $[Tp^{Me2}Ir(=CH-CH_3)(H)(PMe_3)]^+$

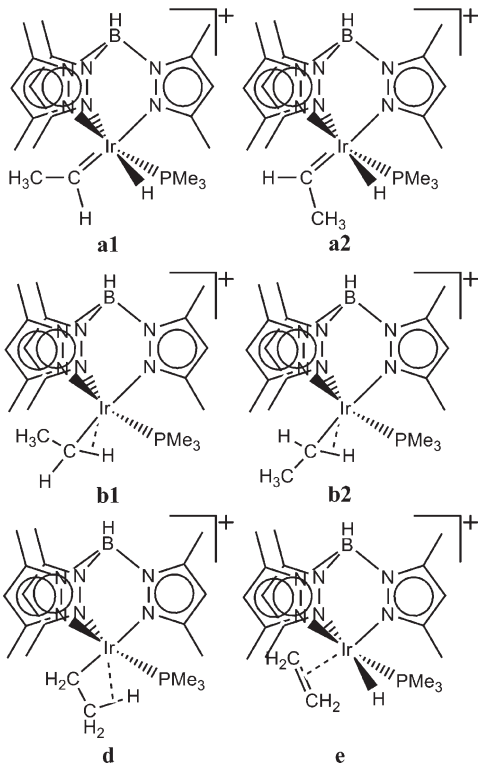

B3LYP is a widely used functional, but its accuracy in the reproduction of π-stacking interactions has been called into question. The problem does not seem to be critical for this system, but the validity of the results was further confirmed by an additional set of geometry optimizations with the hybrid meta-GGA functional MPWB1K.[55] The key energy barriers were slightly reduced with MPWB1K, but the trends were completely unchanged. For the Tp^{Me_2} system, the gas-phase B3LYP value of 17.9 kcal·mol^{-1} for $\Delta^{‡}E°_{298}$ was reduced to 13.7 kcal·mol^{-1} with MPWB1K, and the corresponding values for the Cp* system were 7.8 and 5.7 kcal·mol^{-1}, respectively.

Results and Discussion

The $[Tp^{Me_2}Ir(=CH-CH_3)(H)(PMe_3)]^+$ System. The optimized minima for this system are shown in Scheme 2 and their energies summarized in Figure 1.

The starting hydride ethylidene species **a** presents two rotamers with close energies (0.8 kcal·mol^{-1}) differing in the orientation of the ethylidene with respect to the Tp^{Me_2}. The geometries of these two minima, **a1** and **a2**, are shown in Scheme 2, and they interconvert through transition state **tsa1a2**, which is 8.0 kcal·mol^{-1} above **a1**.

Hydrogen migration from iridium to the α-carbon of the ethylidene yields the alkyl complex $[Tp^{Me_2}Ir(CH_2-CH_3)(PMe_3)]^+$. In this case, the α- and β-agostic complexes were found, but nonagostic species were not located. There are two α-agostic complexes, **b1** and **b2**, that are connected to **a1** and **a2**, respectively. Their energies are 15.0 and 16.6 kcal·mol^{-1} above **a1**, respectively. The agostic nature of these complexes manifests itself in the lengthening of the α-agostic bond (1.112 Å in **b1**; 1.163 Å in **b2**) and the decrease

(42) Frisch, M. J.; Trucks, G. W.; Schlegel, H. B.; Scuseria, G. E.; Robb, M. A.; Cheeseman, J. R.; Montgomery, J. A., Jr.; Vreven, T.; Kudin, K. N.; Burant, J. C.; Millam, J. M.; Iyengar, S. S.; Tomasi, J.; Barone, V.; Mennucci, B.; Cossi, M.; Scalmani, G.; Rega, N.; Petersson, G. A.; Nakatsuji, H.; Hada, M.; Ehara, M.; Toyota, K.; Fukuda, R.; Hasegawa, J.; Ishida, M.; Nakajima, T.; Honda, Y.; Kitao, O.; Nakai, H.; Klene, M.; Li, X.; Knox, J. E.; Hratchian, H. P.; Cross, J. B.; Bakken, V.; Adamo, C.; Jaramillo, J.; Gomperts, R.; Stratmann, R. E.; Yazyev, O.; Austin, A. J.; Cammi, R.; Pomelli, C.; Ochterski, J. W.; Ayala, P. Y.; Morokuma, K.; Voth, G. A.; Salvador, P.; Dannenberg, J. J.; Zakrzewski, V. G.; Dapprich, S.; Daniels, A. D.; Strain, M. C.; Farkas, O.; Malick, D. K.; Rabuck, A. D.; Raghavachari, K.; Foresman, J. B.; Ortiz, J. V.; Cui, Q.; Baboul, A. G.; Clifford, S.; Cioslowski, J.; Stefanov, B. B.; Liu, G.; Liashenko, A.; Piskorz, P.; Komaromi, I.; Martin, R. L.; Fox, D. J.; Keith, T.; Al-Laham, M. A.; Peng, C. Y.; Nanayakkara, A.; Challacombe, M.; Gill, P. M. W.; Johnson, B.; Chen, W.; Wong, M. W.; Gonzalez, C.; Pople, J. A. *Gaussian 03, Revision C.02 ed.*; Gaussian, Inc.: Wallingford, CT, 2004.
(43) Francl, M. M.; Pietro, W. J.; Hehre, W. J.; Binkley, J. S.; Gordon, M. S.; Defrees, D. J.; Pople, J. A. *J. Chem. Phys.* **1982**, *77*, 3654–3665.
(44) Hariharan, P. C.; Pople, J. A. *Theor. Chim. Acta* **1973**, *28*, 213–222.
(45) Hehre, W. J.; Ditchfield, R.; Pople, J. A. *J. Chem. Phys.* **1972**, *56*, 2257.
(46) Ehlers, A. W.; Bohme, M.; Dapprich, S.; Gobbi, A.; Hollwarth, A.; Jonas, V.; Kohler, K. F.; Stegmann, R.; Veldkamp, A.; Frenking, G. *Chem. Phys. Lett.* **1993**, *208*, 111–114.
(47) Hay, P. J.; Wadt, W. R. *J. Chem. Phys.* **1985**, *82*, 299–310.
(48) Roy, L. E.; Hay, P. J.; Martin, R. L. *J. Chem. Theory Comput.* **2008**, *4*, 1029–1031.
(49) Hay, P. J.; Wadt, W. R. *J. Chem. Phys.* **1985**, *82*, 270–283.
(50) Wadt, W. R.; Hay, P. J. *J. Chem. Phys.* **1985**, *82*, 284–298.
(51) Cances, E.; Mennucci, B.; Tomasi, J. *J. Chem. Phys.* **1997**, *107*, 3032–3041.
(52) Cossi, M.; Barone, V.; Mennucci, B.; Tomasi, J. *Chem. Phys. Lett.* **1998**, *286*, 253–260.
(53) Mennucci, B.; Tomasi, J. *J. Chem. Phys.* **1997**, *106*, 5151–5158.
(54) Miertus, S.; Tomasi, J. *Chem. Phys.* **1982**, *65*, 239–245.
(55) Zhao, Y.; Truhlar, D. G. *J. Phys. Chem. A* **2004**, *108*, 6908–6918.

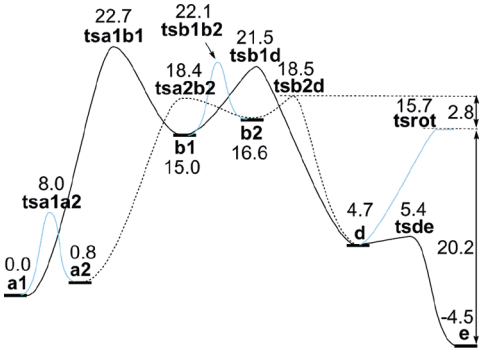

Figure 1. Gibbs energy profile for the transformation from **a1** and **a2** to **e**. ΔG°_{298} values are in kcal·mol^{-1}.

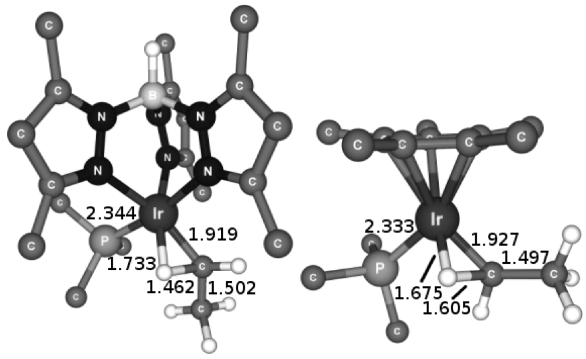

Figure 2. Optimized geometries of complexes **tsa2b2** (left) and **tsA1B** (right). Selected distances are given in Å. Most hydrogen atoms of the Tp^{Me_2}, Cp*, and PMe_3 ligands have been removed for clarity.

of Ir−C−H angle (98.9° in **b1**; 79.8° in **b2**). **b2** is the least stable but shows the strongest agostic deformation. This complex has the most favorable arrangement from the electronic point of view, but unfavorable steric repulsions between the phosphine and the alkyl groups. The alkyl complex **d** presents a β-agostic geometry. This species is much more stable than **b1** and **b2**, being only 4.7 kcal·mol^{-1} above **a1**. **d** has a very long C^β−H distance of 1.227 Å and a short Ir−H bond length of 1.803 Å. There is no other isomer of **d**, which is connected to both **b1** and **b2**.

The reaction product **e** presents a geometry similar to **d**, where the ethene is twisted, avoiding the sterical bulk of Tp^{Me_2}. The computed overall exergonicity from **a1** to **e** is 4.5 kcal·mol^{-1}. This value is also in reasonable agreement with the experimentally estimated exergonicity of 8 kcal·mol^{-1} (please notice that the experimental estimation is obtained from a measured $\Delta^\ddagger G^\circ_{226}$ of 16.7 kcal·mol^{-1} for the direct process and a measured $\Delta^\ddagger G^\circ_{298}$ of 25.1 kcal·mol^{-1} for the reverse reaction, assuming a small temperature dependence of $\Delta^\ddagger G^\circ$).

The energies of the transition states interconnecting species **a**, **b**, **d**, and **e** are shown in Figure 1. Since the α-agostic species **b1** and **b2** are by far the highest-energy intermediates, their associated transition states are also high in energy, and the corresponding reaction steps are rate-determining. The barriers are lower for the transition states associated with **b2**, **tsa2b2**, and **tsb2d**, with energies of 18.4 and 18.5 kcal·mol^{-1} relative to **a1** in both cases. The structure for species **tsa2b2**, in Figure 2, agrees with the expected concerted formation of the C−H (1.462 Å) bond and cleavage of Ir−H (1.733 Å) and Ir=C (1.919 Å) bonds. The path through **b2** is very smooth, because the transition states are only 2 kcal·mol^{-1} above this intermediate. Transition states associated with **b1** are higher in energy (22.7, 21.5 kcal·mol^{-1}) because of the steric bulk of methyl substituents on the ligands. Our hydride migration barrier (**tsa2b2**) is in agreement with the barrier of 17.6 kcal·mol^{-1} computed for the same process on the bidentate system Tp^{Me_2}Ir(H)(*o*-C_6H_4(O)C(CH_3)=).[27] The transition state **tsde**, connecting the β-agostic alkyl complex **d** and product **e**, has a relative energy of only 5.4 kcal·mol^{-1} and is just 0.7 kcal·mol^{-1} above **d**.

The lowest-energy reaction pathway from the hydride−alkylidene complex **a1** to the hydride−alkene complex **e** goes through species **tsa1a2**, **a2**, **tsa2b2**, **b2**, **tsb2d**, **d**, and **tsde** (see Figure 1). This process has an overall barrier $\Delta^\ddagger G^\circ_{298}$ of 18.5 kcal·mol^{-1}, which is in excellent agreement with the experimentally measured $\Delta^\ddagger G^\circ_{226}$ of 16.7 kcal·mol^{-1}. The highest-energy transition state **tsb2d**, which corresponds to the conversion from the α-agostic intermediate to the β-agostic one, is nearly equal in energy to the transition state **tsa2b2** corresponding to the hydride migration. The $\Delta^\ddagger G^\circ_{298}$ value of 23.0 kcal·mol^{-1} computed for the reverse, **e** → **a**, process is slightly lower but in good agreement with the experimentally measured value of $\Delta^\ddagger G^\circ_{298}$ of 25.1 kcal·mol^{-1}.

There is a serious difference in the experimental assignment of the barrier from **e** to **d**.[34] It was estimated experimentally to be $\Delta^\ddagger G^\circ_{273}$ 21.1 kcal·mol^{-1} relative to **e**, while in our calculations **tsde** is only 9.9 kcal·mol^{-1} above **e** (at 298 K). However, this discrepancy can be easily explained taking into account that the experiment measured the rate of scrambling between a deuterated alkene and the hydride in **e**. This scrambling obviously requires the conversion from **e** to **d** through **tsde**, but it also requires the internal rotation of the β-methyl of the alkyl to make its hydrogens equivalent. The computed transition state **tsrot** for this second process is 20.2 kcal·mol^{-1} above **e**. Thus, agreement with all measured experimental barriers was accomplished, providing strong support for the proposed mechanism.

A hypothetical alternative mechanism, the direct 1,2-hydrogen shift within the hydrocarbon ligand, i.e., without metal participation, was discarded, since the corresponding computed transition state is at 34.4 kcal·mol^{-1} above **a1** in terms of $\Delta^\ddagger G^\circ_{298}$ in the gas phase, which is prohibitively high. A similar behavior was reported previously for the Tp^{Me_2}Ir(H)(*o*-C_6H_4(O)C(CH_3)=) system.[27]

The [Cp*Ir(=CH−CH_3)(H)(PMe_3)]$^+$ System. [Cp*Ir(=CH−CH_3)(H)(PMe_3)]$^+$, obtained by protonation of the [Cp*Ir(CH=CH_2)(H)(PMe_3)], also yields a hydride−alkene complex. However, in this case no intermediates were experimentally detected at −80 °C, indicating an overall reaction faster than in the previously studied system.[13]

The computed local minima are presented in Scheme 3, and their energies are given in Figure 3. Qualitatively, this system is similar to the [Tp^{Me_2}Ir(=CH−CH_3)(H)(PMe_3)]$^+$ one. Thus, it will be discussed in less detail, highlighting only the differences. The α-agostic (**B**) and the nonagostic (**C**) alkyl complexes are 0.4 and 1.0 kcal·mol^{-1} above **A1**, respectively, while the β-agostic (**D**) is 0.3 kcal·mol^{-1} below **A1**. In the nonagostic species **C** the Ir−C−H angle is 107.3° as compared with 100.6° in the α-agostic complex **B**. The product **E** is connected directly only to **D** and has an energy 13.6 kcal·mol^{-1} below **A1**. The transition state connecting the alkyl **D** to **E** has an energy 1.4 kcal·mol^{-1} below that of **D** on the ΔG°_{298} scale, which means that the **D** → **E** conversion is barrierless at room temperature.

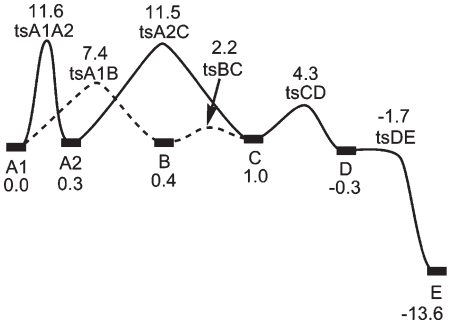

Figure 3. Gibbs energy profile for the transformation from **A1** and **A2** to **E**. ΔG°_{298} values are in kcal·mol^{-1}.

Scheme 3. Schematic Representation of the Rearrangement of the Hydride−Ethylidene Complex [Cp*Ir(=CH−CH$_3$)(H)(PMe$_3$)]$^+$

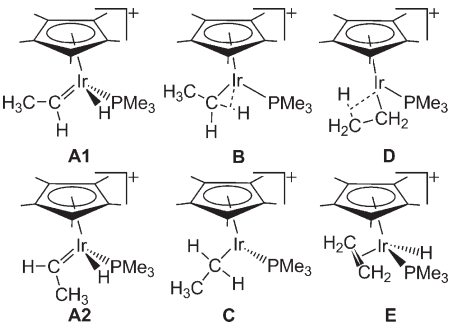

The preferred reaction pathway from **A1** to **E** goes through intermediates **B**, **C**, and **D**. The rate-limiting step is the α-H migration through transition state **tsA1B** (see Figure 2), with a barrier of only 7.4 kcal·mol^{-1} above **A1**. The C−H, Ir−C, and Ir−H distances of 1.605, 1.927, and 1.675 Å, respectively, are consistent with the fact that **tsA1B** is a transition state for hydride migration. The low barrier is in full agreement with the experimental observation of a fast process. From **A2** there are two reaction pathways with similar barriers slightly above 11 kcal·mol^{-1}, via **C** or via **A1** formation.

Similarly to the [Tp^{Me_2}Ir(=CH−CH$_3$)(H)(PMe$_3$)]$^+$ system, the direct 1,2-hydrogen shift without metal participation has a prohibitively high $\Delta^{\ddagger}G^{\circ}_{298}$ barrier of 35.1 kcal·mol^{-1} in the gas phase.

Comparison between the [Tp^{Me_2}Ir(=CH−CH$_3$)(H)(PMe$_3$)]$^+$ and [Cp*Ir(=CH−CH$_3$)(H)(PMe$_3$)]$^+$ Systems. For the system with Tp^{Me_2}, the highest-energy transition state **tsb2d** corresponds to the conversion from the α-agostic to the *β*-agostic intermediate, although the transition state **tsa2b2** for the hydride migration is located only 0.1 kcal·mol^{-1} below. For the system with Cp*, the rate-limiting step corresponds to the hydride migration through transition state **tsA1B**. There is a change in the rate-limiting step between the two systems, but this seems to have little chemical relevance.

The critical difference between the two systems, which affects the chemical behavior, is the barrier between the reactant and the rate-determining transition state. The value is 18.5 kcal·mol^{-1} for the Tp^{Me_2} system and 7.4 kcal·mol^{-1} for the Cp* system, with a difference of about 10 kcal·mol^{-1}. Interestingly, the barriers for the inverse reaction, which would be endergonic, are much closer, with values of 23.0 and 21.0 kcal·mol^{-1}, respectively. Comparison of reaction

Scheme 4. Energy Decomposition for the Formation of Compounds a1 and A1 from the Fragments CHCH$_3$ and [Tp^{Me2}IrH(PMe$_3$)]$^+$ or [Cp*IrH(PMe$_3$)]$^+$[a]

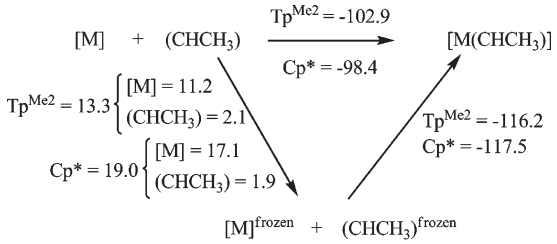

[M] = [Tp^{Me2}IrH(PMe$_3$)]$^+$ and [Cp*IrH(PMe$_3$)]$^+$

[a] The values presented are potential energies without ZPE correction in kcal·mol^{-1}.

profiles (Figures 1 and 3) clearly shows that the main difference between the two systems is in the relative energies of the starting species, **a**/**A**: with reference to **e**/**E**, **a1** and **a2** have a much lower energy in the Tp^{Me_2} system than **A1** and **A2** in the Cp* system. This is, for instance, reflected in ΔG°_{298} for the entire process (**a**/**A** → **e**/**E**), which is −4.5 kcal·mol^{-1} for the Tp^{Me_2} system and −13.6 kcal·mol^{-1} for the Cp* system.

The role of steric effects in the reactivity of the system was further elucidated by additional calculations, in which **a**, **e**, **A**, and **E** were reoptimized after replacing the methyls of the Tp^{Me_2}, Cp*, and PMe$_3$ ligands by hydrogen atoms. These species with Tp, Cp, and PH$_3$ ligands are labeled as **a**−**h**, **e**−**h**, **A**−**h**, and **E**−**h**. The difference in energy between **a**−**h** and **e**−**h** is −10.4 kcal·mol^{-1} (**a**−**e** −4.5 kcal·mol^{-1}); that between **A**−**h** and **E**−**h** is −9.2 kcal·mol^{-1} (**A**−**E** −13.6 kcal·mol^{-1}). Therefore, suppression of steric effects makes the systems much more similar. Without steric effects the reaction would become slightly more exergonic (1.2 kcal·mol^{-1}) for the Tp-derived ligand, as could be expected from purely electronic effects.[38]

To further analyze the difference in stability between the two metal−alkylidene complexes **a1** and **A1**, the metal−carbene binding energy was computed for both species and decomposed in distortion and interaction terms, following an approach already employed by some of us to investigate different coordination modes of one ligand.[27,56] The binding energy that results from the formation of complexes **a1** and **A1** from the fragments ([Tp^{Me_2}IrH(PMe$_3$)]$^+$ or [Cp*IrH(PMe$_3$)]$^+$ and CHCH$_3$) in their optimized isolated geometries has been determined as arising from the combination of two terms. One is the distortion of the fragments from their free geometries to those they adopt in the complexes (ΔE_{dist}) and the other the interaction energy that stems from the combination of the two fragments to give the real complexes (ΔE_{inter}). The results are summarized in Scheme 4. The alkylidene is strongly bonded in both systems,[57] as shown by the high values of the binding energies (102.9 and 98.4 kcal·mol^{-1} for the Tp^{Me_2} and Cp* complexes, respectively). In agreement with the higher stability of the metal−alkylidene in the Tp^{Me_2} complex, the M=C bond energy of the Tp^{Me_2} system **a1** is 4.5 kcal·mol^{-1} larger than that of the Cp* system **A1**. This difference is mainly retrieved in the distortion term of the metal fragment since this

(56) Falvello, L. R.; Gines, J. C.; Carbó, J. J.; Lledós, A.; Navarro, R.; Soler, T.; Urriolabeitia, E. P. *Inorg. Chem.* **2006**, *45*, 6803–6815.
(57) Frenking, G.; Solà, M.; Vyboishchikov, S. F. *J. Organomet. Chem.* **2005**, *690*, 6178–6294.

Scheme 5. Representation of the Steric Effects Caused by the Alkylidene (top, left), Alkene (top, right), Tp^{Me2} (bottom, left), and Cp* Ligands (bottom, right); See Text

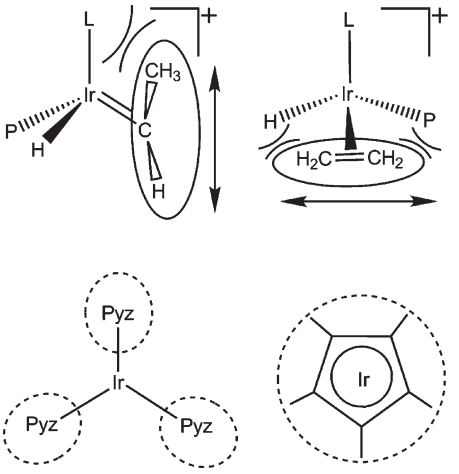

destabilizing term is 5.9 kcal·mol^{-1} lower in **a1** (11.2 kcal·mol^{-1}) than in **A1** (17.1 kcal·mol^{-1}). Thus, the different behavior can be attributed to steric effects. In contrast, the interaction energy between the distorted fragments, more easily related to electronic effects, is very similar in both complexes (−116.2 and −117.7 kcal·mol^{-1} in **a1** and **A1**, respectively). An alternative explanation could be that the M=C bond is stronger in the Tp^{Me_2} system, as the Ir−N bonds of the Tp^{Me_2} are weaker than the Ir−C bonds in the Cp*. We repeated the same type of analysis for all other systems considered (**e**/**E**, **a**−**h**/**A**−**h**, and **e**−**h**/**E**−**h**), the results being collected in Scheme S1 in the Supporting Information. Interestingly, **a1**/**A1** is the only pair where the bond with the Tp^{Me_2} ligand is stronger than with Cp*, confirming once again the suitability of the combination between Tp^{Me_2} and =$CHCH_3$ to stabilize the metal−carbene isomer.

Inspection of the geometries gives some hints about the different steric requirements of alkylidene and ethylene ligands. Those of the alkylidene manifest preferentially in a direction parallel to the Ir−Tp or Ir−Cp axis, while for ethylene they appear mostly in a direction perpendicular to the Ir−Tp or Ir−Cp axis (see Scheme 5). This makes the alkylidene fit better on the Tp^{Me_2} system than the alkene. The Tp^{Me_2} puts steric pressure in the three precise directions of the N substituents, while Cp* has a uniform although lower steric pressure. The stronger preference of the Tp^{Me_2} system for octahedral environments[35,58] can also be related to these steric considerations.

The steric requirements in the rest of the complexes fit better with the Cp* pattern because the steric pressure of the ligands is not concentrated in a specific region. For instance, the transition state **tsab** presents the hydride approaching the alkylidene to form **b**, a movement sterically hindered because of the proximity of the hanging methyls of Tp^{Me_2}. The case of the β-agostic complexes **d**/**D** is somewhat special because of the more compact arrangement of the ligand. In this case, the relative energies with respect to the reactants are more similar (4.7 kcal·mol^{-1} for **d** → **a1**, −0.3 kcal·mol^{-1} for **D** → **A1**).

Conclusions

Our computational study on the ligand rearrangement in the $[Tp^{Me_2}Ir(=CH-CH_3)(H)(PMe_3)]^+$ and $[Cp^*Ir(=CH-CH_3)(H)(PMe_3)]^+$ systems reproduces accurately the available experimental kinetic data on the reactivity of these species. The results confirm the validity of the previously proposed mechanism involving active participation of the hydride ligand and going through intermediates containing alkyl ligands stabilized by agostic interactions. The computed barriers are 18.5 and 7.4 kcal·mol^{-1}, respectively, indicating a much faster reaction for the $[Cp^*Ir(=CH-CH_3)(H)(PMe_3)]^+$ system, in agreement with experiment.

The different reaction rates for the two complexes can be attributed to differences in steric effects and flexibility. Tp^{Me_2} presents the pyrazolyl methyl groups close to the other ligands, hindering addition of the α-H bond and alkyl rotation. At the same time, the space between the methyl groups is sufficient to accommodate the alkylidene ligand, thus stabilizing the reactant complex. The steric effect of the Cp* is more uniform in space and conserved throughout the process. The electronic effects seem to play a minor role in the difference between these systems.

Acknowledgment. We thank the ICIQ Foundation, the Spanish Ministerio de Ciencia e Innovacion (Consolider Ingenio 2010 CSD2006-0003 and CSD2007-000006; projects CTQ2007-62814, CTQ2008-06866-CO2-01/BQU, CTQ2008-06866-CO2-02/BQU, and CTQ2008-03077/BQU, FEDER support), Generalitat de Catalunya (grants 2009SGR0259 and XRQTC), and Junta de Andalucia (project numbers FQM-315 and FQM-67). M.B. thanks the Spanish Ministerio de Ciencia e Innovacion for a "Juan de la Cierva" grant.

Supporting Information Available: Scheme S1, Cartesian coordinates, and absolute energies of all presented species are available free of charge via the Internet at http://pubs.acs.org.

(58) Ruba, E.; Simanko, W.; Mereiter, K.; Schmid, R.; Kirchner, K. *Inorg. Chem.* **2000**, *39*, 382–384.